

## Resonant ion-pair formation in the recombination of $\text{NO}^+$ with electrons: Cross-section determination

A. Le Padellec,<sup>1</sup> N. Djurić,<sup>2</sup> A. Al-Khalili,<sup>3</sup> H. Danared,<sup>4</sup> A. M. Derkach,<sup>3</sup> A. Neau,<sup>3</sup> D. B. Popović,<sup>2</sup> S. Rosén,<sup>3</sup>  
J. Semaniak,<sup>5</sup> R. Thomas,<sup>3,6</sup> M. af Ugglas,<sup>4</sup> W. Zong,<sup>2,3</sup> and M. Larsson<sup>3</sup>

<sup>1</sup>*Le Laboratoire Collision Agrégats Reactivité, UMR 5589 Université Paul Sabatier-Toulouse III 118, route de Narbonne Bâtiment III  
R1, b4 31062 Toulouse Cedex 4, France*

<sup>2</sup>*JILA, University of Colorado and National Institute of Standards and Technology, Boulder, Colorado 80309-0440*

<sup>3</sup>*Department of Physics, Stockholm University, Box 6730, S-113 85 Stockholm, Sweden*

<sup>4</sup>*Manne Siegbahn Laboratory, Stockholm University, S-104 05 Stockholm, Sweden*

<sup>5</sup>*Institute of Physics, Pedagogical University, 25-430 Kielce, Poland*

<sup>6</sup>*FOM Instituut AMOLF, Kruislaan 407, 1098 SJ Amsterdam, The Netherlands*

(Received 5 September 2000; published 30 May 2001)

Resonant ion-pair formation from the collisions of  $\text{NO}^+$  ions with electrons was studied using the heavy-ion storage ring CRYRING at the Manne Siegbahn Laboratory of Stockholm University. The total cross section is measured for the formation of  $\text{N}^+ + \text{O}^-$  for electron energies 8–18 eV, and the results are compared with ion-pair formation in photoionization work. A peak in the cross section is observed at 12.5 eV, with a magnitude of  $8.5 \times 10^{-19} \text{ cm}^2$ . An attempt to extract the cross section for the reverse process of associative ionization is made.

DOI: 10.1103/PhysRevA.64.012702

PACS number(s): 34.80.Ht, 34.50.Gb

### I. INTRODUCTION

Dissociative recombination (DR) is a process in which a molecular ion  $AB^+$  captures an electron followed by molecular dissociation into neutral fragments. Resonant ion-pair formation (RIP) proceeds very much in the same way, the difference being that charged species rather than neutral species are formed, which means that the number of positive and negative charges is preserved. In most cases the RIP process is endothermic (one exception being  $\text{HF}^+$  [1]). As a result, the cross section exhibits a threshold behavior. For a diatomic ion, the ion-pair formation can be represented by  $AB^+ + e^- \rightarrow AB^{**} \rightarrow A^+ + B^- + \text{KER}$ , where KER is the kinetic energy release.

The  $\text{NO}^+$  ion, together with  $\text{N}_2^+$  and  $\text{O}_2^+$ , is very important in the terrestrial ionosphere where dissociative recombination and photodissociation are the only chemical loss processes. The resulting energetic oxygen atoms give rise to atmospheric phenomena such as the geocorona [2]. The DR process of  $\text{NO}^+$  with electrons has been studied both experimentally and theoretically. The experimental studies include the ion-trap experiment (Walls and Dunn [3]), the merged-beams experiment (Mul and McGowan [4]), the flowing afterglow experiments (Alge *et al.* [5], Mostefaoui *et al.* [6]), the stationary afterglow experiment (Weller and Biondi [7]), and more recent studies using the storage ring ASTRID at Aarhus University (Vejby-Christensen *et al.* [8]). These various experiments concerned different aspects of the DR process—cross sections or thermal rate coefficients versus center-of-mass energy or electron temperature, respectively, and there is a very good agreement between the different experiments, with the thermal-rate coefficient at room temperature within the range of  $4-5 \times 10^{-7} \text{ cm}^3 \text{ s}^{-1}$ . This is also in very good agreement with the theoretical computations found in the pioneering work of Bardsley [9] and Lee [10]

and the more recent work of Sun *et al.* [11]. To the best of our knowledge, a similar investigation concerning the RIP process had not been performed prior to this work, neither experimentally nor theoretically. The reverse process to DR, namely the associative ionization (AI) between N and O neutrals, has also received some attention [12,13], and some quantum yields were measured as a function of the quantum states of the associating atoms. On the other hand, there is still a lack of data for similar measurements concerning the ionic counterpart, i.e., associative ionization in  $\text{N}^+ + \text{O}^-$  collisions, which is the reverse process to RIP.

This paper presents our storage ring results on resonant ion-pair formation from ground-state  $\text{NO}^+$  ions. In addition, a model is used to derive information concerning the reverse process, the associative ionization. The paper is organized as follows: the general features of the storage ring are introduced (Sec. II) as well as the data analysis procedure to extract the RIP cross sections (Sec. III). These cross sections are presented, discussed, and put in perspective with those reported by others (Sec. IV). A model is used to extract the AI cross sections in Sec. V.

### II. EXPERIMENT

The experiment was performed at the heavy-ion storage ring CRYRING, located at the Manne Siegbahn Laboratory of Stockholm University. A brief description is given below (see also Fig. 1).

The  $\text{NO}^+$  ions are produced in a hollow cathode cold plasma ion source called JIMIS [14] by simply letting air leak in. After extraction from the source at 40 keV, the ions are mass selected, injected into the ring, and accelerated to the 3.2 MeV maximum energy (limited by the magnetic rigidity of the ring), which takes about 1 s. This time scale allows infrared active ions, such as  $\text{NO}^+$  (with a sizable dipole moment), to vibrationally relax prior to measurements. For  $\text{NO}^+$ , the radiative lifetimes for the lowest  $X^1\Sigma^+$  vibrational levels are less than 100 ms [15], whereas those for the

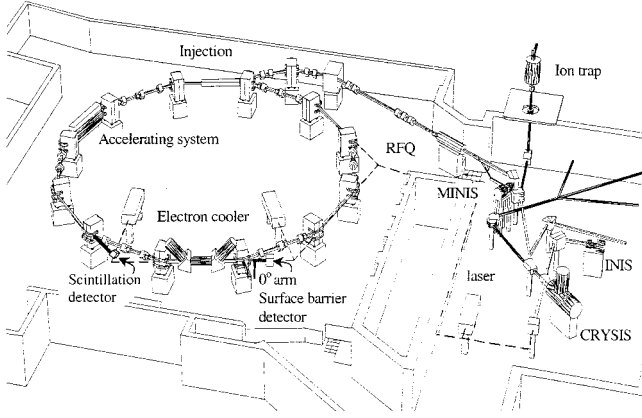


FIG. 1. The ion storage ring CRYRING at the Manne Siegbahn Laboratory, Stockholm University.

a  $^3\Sigma^+$  metastable state are about 700 ms [16]. In any case, these are much shorter lifetimes than the acceleration time (1.1 s) and the storage time before data are taken, which is 3 s after full energy has been reached. In the electron cooler section, the ion beam is merged with a collinear, quasimonoenergetic electron beam. These electrons have a velocity spread that can be described by an anisotropic Maxwell-Boltzmann distribution (in the rest frame of the electrons):

$$F(\mathbf{v}_e) = \frac{m_e}{2\pi kT_{e\perp}} \left( \frac{m_e}{2\pi kT_{e\parallel}} \right)^{1/2} \exp\left( -\frac{m_e v_{e\perp}^2}{2kT_{e\perp}} - \frac{m_e v_{e\parallel}^2}{2kT_{e\parallel}} \right), \quad (1)$$

where  $T_{e\parallel}$  and  $T_{e\perp}$  represent the longitudinal and transverse temperatures, respectively, with  $kT_{e\parallel} \approx 0.1$  meV and  $kT_{e\perp} \approx 1$  meV.

The experimental protocol [17] is the following. First, the ions are accelerated and then cooled for 3 s by allowing them to interact with velocity matched electrons, which results in a reduction of their thermal random motion (phase-space cooling); in this particular case the phase-space cooling is slow and the primary reason for the 3 s cooling is to remove the metastable state and to obtain vibrational cooling. Second, the electron velocity is changed so that collisions at well-defined energies are obtained. The center-of-mass energy is given by the conventional relation

$$E_{c.m.} = (\sqrt{E_e} - \sqrt{E_{cool}})^2, \quad (2)$$

with  $E_e$  the average electron energy and  $E_{cool}$  the cooling electron energy ( $\approx 60$  eV in the present case), both energies expressed in the laboratory frame of reference. For each injection cycle, just after the cooling period, the cathode voltage of the electron cooler is rapidly detuned to about 110 V (in about 2 ms), which corresponds roughly to 7.5 eV in the center-of-mass frame. This voltage is further increased for 2 s to reach the top value of  $\approx 150$  V ( $\approx 20$  eV center of mass) in order to cover the energy range of interest for the process under study. Then, the voltage is rapidly ramped down to the cooling value in about 2 ms, and the injection cycle is completed with the electron beam at cooling energy for an additional 3.6 s. The cathode voltage variation scheme is shown

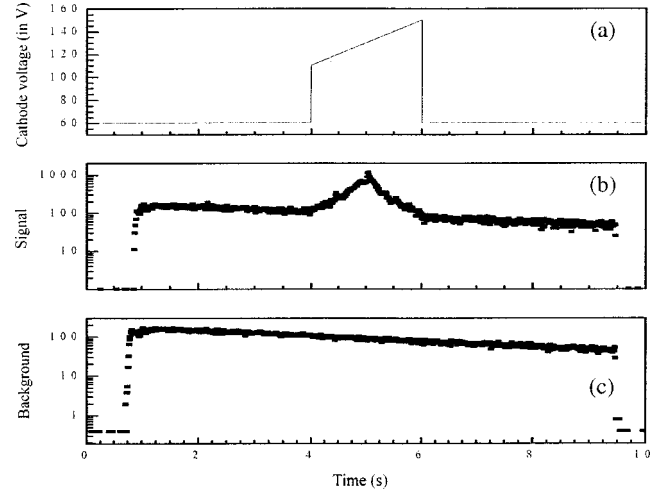


FIG. 2. (a) The electron cooler cathode voltage variation scheme versus time. (b) RIP signal+background spectrum measured versus time by means of the surface barrier detector. (c) Background spectrum measured versus time by means of the surface barrier detector.

in Fig. 2. The energy resolution at 10-eV center-of-mass energy is under optimal conditions about 125 meV (mainly due to the energy spread in the electron beam), and the absolute accuracy of the energy scale is about 50 meV. As will follow later, we most probably did not have optimal conditions in the present experiment.

While the ions are circulating in the main orbit, the negatively charged products  $O^-$  from the RIP process, and  $O^-$  produced from  $NO^+$  collisions with the rest gas molecules, are bent to the outside of the main trajectory, where they hit an energy-sensitive 27-mm-diam surface barrier detector (SBD), which has a 100% detection efficiency at the chosen beam energy. The  $O^-$  products are spread over an area corresponding to about one-third of the detector area. The SBD is placed in the dipole chamber, just downstream of the electron cooler. The  $O^-$  signal is recorded by a multichannel scaler (MCS), which gives the number of counts in the detector versus both time (Fig. 2) and cathode voltage and, by simple correlation, versus the center-of-mass energy. However, as mentioned earlier, part of the detected  $O^-$  fragments arises from collisions with the rest gas molecules and has to be separated from the true signal.

As shown in Fig. 1, a scintillation detector is mounted at the end of one of the straight sections. Neutral particles arising from collisions of the stored ion beam with residual gas molecules are recorded by this detector during the experiment, hence it serves as a convenient beam intensity monitor.

### III. DATA ANALYSIS PROCEDURE TO EXTRACT THE CROSS SECTION

The experimental resonant ion-pair formation rate coefficient  $\langle \nu_{c.m.} \sigma \rangle$  is given by the relation (for a given center-of-mass velocity  $\nu_{c.m.}$ ) [18,19]

$$\langle \nu_{c.m.} \sigma \rangle = R_B \frac{C}{n_e l} \frac{N_{RIP}}{N_{Sci}} \quad (3)$$

where  $C$  is the circumference of the ring,  $l$  the length of the electron cooler, and  $n_e$  the electron density.  $N_{\text{RIP}}$  represents the number of counts coming from the RIP process in a certain time interval; it is obtained by subtracting the background counts (arising from collisions with residual gas molecules) measured in the SBD with the electron cooler set at cooling energy from the number of counts in the SBD when the cathode voltage is ramped. Simultaneously with the recording of the SBD MCS spectra with the cathode voltage ramped, the scintillation detector was used to record the number of neutral particles  $N_{\text{Sci}}$ , arising from collisions of the stored ion beam with rest gas molecules. The last term in Eq. (3) to be discussed is  $R_B$ , which is the destruction rate per ion and per unit time in the straight section containing the scintillation detector. It is obtained by measuring a MCS spectrum from the scintillation detector simultaneously with measuring the ion-beam current by means of a current transformer. It is directly related to the number of counts measured in the scintillation detector per unit time,  $d(N_{\text{Sci}})/dt$ , thus

$$R_B = \frac{d(N_{\text{Sci}})}{dt} \frac{1}{I_i} S_f e, \quad (4)$$

where  $I_i$  is the ion-beam current recorded by the current transformer,  $e$  is the electric charge, and  $S_f$  is the revolution frequency of the ions, the so-called Shottky frequency. The measured rate coefficient  $\langle v_{\text{c.m.}} \sigma \rangle$  is then related to the cross section by

$$\langle v_{\text{c.m.}} \sigma \rangle = \int_{-\infty}^{+\infty} v \sigma(v) f(v_{\text{c.m.}}, \mathbf{v}_e) d\mathbf{v}_e \quad (5)$$

where  $f(v_{\text{c.m.}}, \mathbf{v}_e)$  is the electron velocity distribution [see Eq. (1)] around the averaged center-of-mass velocity  $v_{\text{c.m.}}$ .

In addition to the analysis procedure described above, a few corrections [14,20] have to be made in order to obtain the rate coefficient (and consequently the cross section) as a function of the electron energy. First, the center-of-mass energy has to be corrected to account for the space charge of the electron beam. In the present case, owing to the weakness of the electron current, this represented a correction of no more than 8–9%. Second, due to the geometry of the electron cooler, the ions do not interact with electrons only in a straight section of the cooler but also in the curved edges where the relative velocity is different. As a result, a number of the counts recorded by the detector at a given energy has a contribution from collisions that occur at somewhat larger center-of-mass energies, resulting in a modification of the signal. An iterative procedure is used for this correction, which has been described previously by Lampert *et al.* [21]. It should be pointed out that this correction is essential in order to determine the correct appearance energy for the RIP process.

#### IV. RESULTS AND DISCUSSION

The absolute cross section for the RIP process as a function of center-of-mass energy is presented in Fig. 3. It was

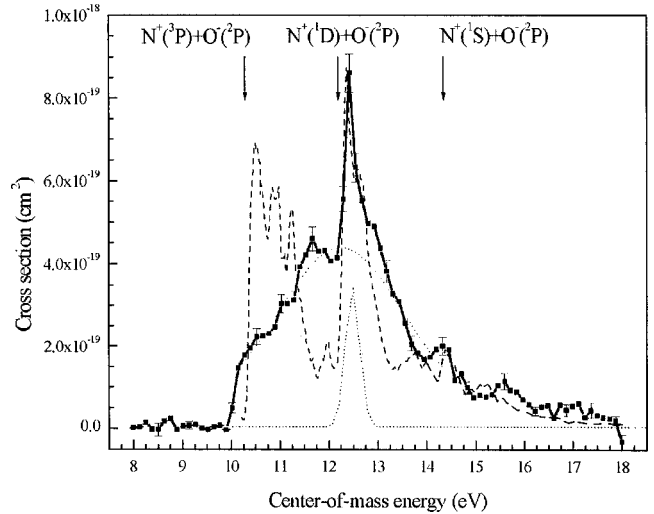


FIG. 3. RIP absolute cross sections are represented versus the center-of-mass energy in by a solid line whereas the normalized photoabsorption data by Erman *et al.* [22] are represented by a dashed line. The error bars are purely statistical at the  $1\sigma$  level. The dotted lines represent the partial RIP cross sections for the two lowest ion-pair limits (see text Sec. V).

measured by recording the  $\text{O}^-$  fragments coming from the  $\text{N}^+ + \text{O}^-(^2P)$  channels. The thresholds for the formation of  $\text{N}^+$  in the  $^3P$ ,  $^1D$ , and  $^1S$  states at 10.3, 12.2, and 14.4 eV [22], respectively, are indicated by the arrows in Fig. 3. Also shown are the data of Erman *et al.* [22] obtained from photoionization of  $\text{NO } X^2\Pi_r$  and leading to the same  $\text{N}^+ + \text{O}^-$  exit channel. The latter data were originally published on a relative scale, but to make the comparison with our data easier, we have normalized them to our largest observed peak at 12.44 eV (571 Å in their wavelength scale). In order to put Erman *et al.* data on our energy scale we used the energy conversion factor  $1 \text{ eV} = 8065.541 \text{ cm}^{-1}$  and the value for  $\text{IP}(\text{NO}) = 9.264 \text{ eV}$  [23].

The RIP cross section for  $\text{NO}^+$  consists of two parts, a broad structure centered about 11.8 eV and a sharp peak at 12.44 eV. At the sharp peak, the magnitude of the cross section is  $8.5 \times 10^{-19} \text{ cm}^2$ . The appearance of  $\text{O}^-$  from RIP occurs at a slightly lower energy (10 eV) than the expected threshold energy at 10.3 eV. This difference of 300 meV is larger than the anticipated resolution of 125 meV and the energy scale accuracy of 50 meV. This disparity might suggest that there is an error in the energy scale, were it not for the excellent agreement between our data and those of Erman *et al.* [22] concerning the peak at 12.44 eV. Thus, a more likely explanation is that the energy resolution in the experiment was 300 meV rather than 125 meV. This could occur if the electron and ion beams were not perfectly aligned. Owing to the electron space-charge effect, the kinetic energy of the electrons in the beam is not uniform over its cross-sectional area. Thus, an ion moving through the electron beam at a finite angle will experience a broader electron-energy distribution than an electron moving parallel with the electron beam.

The discussion that follows will be relatively speculative, due to the sparse amount of molecular data available, espe-

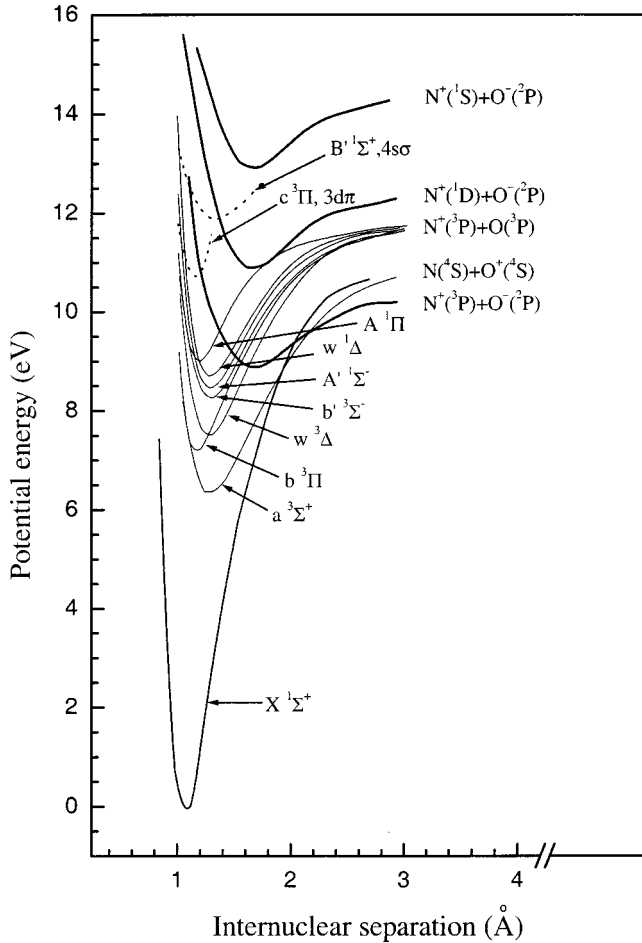


FIG. 4. Ionic and neutral potential curves relevant to the present study. (Adopted from Ref. [22].) The eight ionic states are represented by solid lines, the two Rydberg neutral states by dotted lines, and the three neutral states correlating to the ionic limits  $N^+ + O^-$  by thick solid lines. The ground-state ionic curve is taken from Ref. [31].

cially as it relates to the potential curves of NO correlating to the  $N^+ + O^-$  limits. According to the correlation rules, 12, 9, and 2 different molecular states correlate to  $N^+(^3P) + O^-(^2P)$ ,  $N^+(^1D) + O^-(^2P)$ , and  $N^+(^1S) + O^-(^2P)$ , respectively. These are the  $^2,4\Sigma^+(1)$ ,  $^2,4\Sigma^-(2)$ ,  $^2,4\Pi(2)$ , and  $^2,4\Delta(1)$  states [the  $N^+(^3P) + O^-(^2P)$  limit] [24],  $^2\Sigma^+(2)$ ,  $^2\Sigma^-(1)$ ,  $^2\Pi(3)$ ,  $^2\Delta(2)$ , and  $^2\Phi(1)$  states [the  $N^+(^1D) + O^-(^2P)$  limit] [24], and  $^2\Sigma^+(1)$  and  $^2\Pi(1)$  states [the  $N^+(^1S) + O^-(^2P)$  limit] [24]. (The numbers in parentheses represent the number of electronic states of that particular symmetry, in accordance with Ref. [24].) Three of these ion-pair states are represented in Fig. 4 (the lowest one of each atomic limit).

A comparison of our RIP data and the photoionization ion-pair data [22,25] reveals that the former contain less structures, with the exception of the peak at 12.44 eV. Especially striking is the absence in our cross-section data of the four resonant structures lying above the first threshold of  $N^+(^3P) + O^-(^2P)$ , but below the second one,  $N^+(^1D) + O^-(^2P)$ . In the paper of Erman *et al.* [22], the authors stressed the important role of the intermediate Rydberg  $c^3\Pi$

states,  $3d\sigma, 3d\pi$  (shown in Fig. 4),  $4p\sigma$ , and  $4p\pi$  for the production of the  $N^+(^3P) + O^-(^2P)$  channel. One obvious difference between the two types of experiments is the lack of selection rules for the electron-impact experiment (RIP). Another difference concerns the equilibrium values of the internuclear separation for the two types of targets (1.063 and 1.151 Å for  $NO^+$  and  $NO$ , respectively). Since both targets were vibrationally cold, the result is that the Franck-Condon regions for the vertical transitions are different and consequently so are the couplings driving the RIP and photoionization ion-pair processes. This might explain the absence of the four resonant structures in our data. On the other hand, the broad structure located around 11.8 eV has essentially no counterpart in the photoionization data.

Present in both experiments, and in perfect agreement, is the sharp structure centered at 12.44 eV and located above the  $N^+(^1D) + O^-(^2P)$  limit. In fact, our structure appears slightly broader than that from the photoionization ion-pair formation work. The structure was attributed by Erman *et al.* [22] to be due to direct dissociation via the second ion-pair state. The broader structure that follows, with a maximum at about 12.5 eV, was assigned to be due to the predissociation of the Rydberg state  $B'^1\Sigma^+ 4s\sigma$  (shown in Fig. 4) by the second ion-pair state.

Finally, in the energy range around the third dissociation limit at 14.4 eV,  $N^+(^1S) + O^-(^2P)$ , we clearly observe a peak in the vicinity of the threshold, but due to the rather poor statistics owing to the low cross section, it is difficult to speculate further. A similar structure was observed in the photoionization experiments [22,25].

## V. SOME PARTIAL CROSS SECTIONS FOR THE ASSOCIATIVE IONIZATION PROCESS

We present now the attempt we have made to extract some cross sections for the associative ionization (AI)



which is the reverse process of the RIP mechanism discussed above. The model is based on the detailed balance (DB) principle.

The basic idea is the following. For a given chemical reaction



if one includes the total degeneracies associated with the angular momenta  $g_i$  ( $i = A, B, C$ , and  $D$ ), one gets the relation

$$p^2 g_A g_B \sigma(p) = p'^2 g_C g_D \sigma_{Re v}(p') \quad (7)$$

with  $p^2 = 2\mu E_{c.m.}$  and  $p'^2 = 2\mu' E'_{c.m.}$ ;  $\mu$  ( $\mu'$ ) and  $E_{c.m.}$  ( $E'_{c.m.}$ ) being the reduced masses of the entrance (exit) channels and the corresponding center-of-mass energies, respectively. For the RIP or AI processes  $AB^+ + e^- \leftrightarrow A^+ + B^-$ , one has also to account for the rotation of the molecular ion  $AB^+$ , with the quantum number  $N$ . The theoretical

treatment of the RIP and AI cross sections is fairly similar (see Urbain [26]), and can be expressed by a development in partial waves of the  $S$  matrix elements ( $k_{c.m.}$  and  $k'_{c.m.}$  are the modules of the wave vectors):

$$\sigma_{\text{RIP}}(k_{c.m.}) = \frac{\pi}{k_{c.m.}^2} |S|^2, \quad (8)$$

$$\sigma_{\text{AI}}(k'_{c.m.}) = \frac{\pi}{k_{c.m.}'^2} \sum_N \sum_v |S^{N,v}|^2 (2N+1). \quad (9)$$

If, for simplification, one makes the assumption that the partial wave elements do not depend much on the rotational degree of freedom, it follows that

$$\sum_N \sum_v |S^{N,v}|^2 (2N+1) \approx \sum_N (2N+1) \sum_v |S^{N,v}|^2. \quad (10)$$

Since

$$|S|^2 = \sum_v |S^{N,v}|^2, \quad (11)$$

there is a simple link between the RIP and AI cross sections, if one takes into account the degeneracies  $g_i = 2J_i + 1$  mentioned above ( $g_e = 2$  for the electron):

$$\sigma_{\text{AI}}(E'_{c.m.}) = \frac{\mu}{\mu'} \frac{E_{c.m.}}{E'_{c.m.}} \frac{g_{AB^+} g_e}{g_A + g_B^-} \sum_0^{N_{\max}} (2N+1) \sigma_{\text{RIP}}(E_{c.m.}). \quad (12)$$

The last term to be quantified is  $N_{\max}$ , which appears in the summation  $\sum_0^{N_{\max}} (2N+1) = (N_{\max} + 1)^2$  and is energy dependent. It is related to the rotational temperature and gives the cutoff beyond which the molecular ion is unbound. This is obtained from the centrifugal distortion of the potential curves

$$U_j(R) = V_0(R) - J(J+1) \frac{\hbar}{2\mu'R^2}. \quad (13)$$

For energies with  $N_{\max} > N_{\max \text{ unbound state}}$ , the effective  $N_{\max}$  is taken to be  $N_{\max \text{ unbound state}}$ . The  $J$  quantum number in Eq. (13) can be connected to the rotational quantum number  $N$  by simple vector construction [24].

Figure 5 presents the associative ionization results for the entrance channels  $\text{N}^+(^3P) + \text{O}^-(^2P)$  and  $\text{N}^+(^1D) + \text{O}^-(^2P)$ , respectively. Again it should be pointed out that the outputs of our model deal with partial associative ionization cross sections. Indeed, in order to test this simple method, we predicted the RIP cross section for  $\text{HeH}^+$ , using as input data the direct measurement of the AI process published by Naji *et al.* [27]. To the best of our knowledge, the RIP cross section for  $\text{HeH}^+$  has not been measured yet, but has been calculated by Larson and Orel [28] using the more sophisticated wave-packet formalism. In terms of magnitude for the cross section, our predictions for  $\text{HeH}^+$  based on the DB principle differed from the wave-packet result of Larson

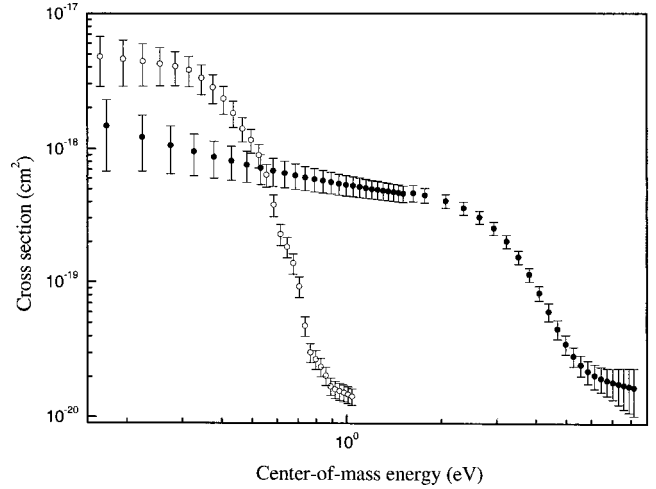


FIG. 5. The extracted AI cross sections versus center-of-mass energy from the DB model (see Sec. V). The closed circles are for the association of  $\text{N}^+(^3P) + \text{O}^-(^2P) \rightarrow \text{NO}^+(X^1\Sigma^+, v=0) + e^-$  whereas the open circles are for  $\text{N}^+(^1D) + \text{O}^-(^2P) \rightarrow \text{NO}^+(X^1\Sigma^+, v=0) + e^-$ .

and Orel [28] by only a factor of 2. A careful error analysis of our model will be given below.

We handled the data in the following way. In our experimental RIP data for  $\text{NO}^+$ , we observed the opening of the three  $\text{N}^+(^3P, ^1D, \text{ and } ^1S) + \text{O}^-(^2P)$  channels. Therefore we had to extract the partial RIP cross sections for these channels in order to apply the DB model. We did so in a somewhat arbitrary way, and we are aware that this can be a matter of discussion. In fact, we considered only the two lowest  $\text{N}^+(^3P \text{ and } ^1D) + \text{O}^-(^2P)$  channels, and fitted our RIP cross sections assuming they consisted of two Gaussians on top of each other (see Fig. 3). Between 10.3 and 12.2 eV, the only channel to be populated is  $\text{N}^+(^3P) + \text{O}^-(^2P)$ . Above 13 eV, both  $^3P$  and  $^1D$  channels certainly do contribute, but it is impossible to know in which proportion. In that respect, our fits certainly underestimate the contribution of the  $^1D$  channel, the corresponding Gaussian being much narrower than that for the  $^3P$  channel. This will certainly contribute to the uncertainties on both the absolute magnitude of the AI cross section and the shape of the curve. These uncertainties constitute an important issue that we develop next. From the different parameters that enter in Eq. (12), we considered the following uncertainties:

First,  $\Delta E_{c.m.}$  and  $\Delta E'_{c.m.}$  for the RIP energy scale (“electron energy”) and the AI energy scale (“ion-pair” energy), respectively. We assumed our RIP energy scale, corrected by the space-charge correction mentioned above, to be accurate within 5%. The following relation links both energy scales:

$$E'_{c.m.} = E_{c.m.} - E_{\text{threshold}}, \quad (14)$$

with  $E_{\text{threshold}}$  representing the RIP thresholds (10.3 and 12.2, respectively). These thresholds are experimental and are assumed to be known within 0.1 eV (using the threshold observed in this experiment, 10.0 eV, would give a 25% smaller AI cross section at 0.1 eV, which is within the error bars given in Fig. 5).

Second, the uncertainty in the cutoff in the rotational quantum number,

$$\Delta N_{\max} = \sqrt{N_{\max}} \approx 15. \quad (15)$$

Third,  $\Delta\sigma_{\text{RIP}}$  represents the experimental uncertainty on the RIP cross sections (see the presentation of the RIP results).

The relation gives the overall AI uncertainties

$$\Delta\sigma_{\text{AI}} = \sigma_{\text{AI}} \left( \frac{\Delta E_{\text{c.m.}}}{E_{\text{c.m.}}} + \frac{[\Delta E_{\text{c.m.}} + \Delta(E_{\text{threshold}})]}{E_{\text{c.m.}} + \Delta E} + 2 \frac{\Delta N_{\max}}{N_{\max} + 1} + \frac{\Delta\sigma_{\text{RIP}}}{\sigma_{\text{RIP}}} \right). \quad (16)$$

The second and third terms on the right-hand side of Eq. (16) contribute the most (at least 60% of the total). Considering these uncertainties, we only show the data above 0.1 eV.

The slope of the curve corresponding to  $\text{N}^+(^3P) + \text{O}^-(^2P) \rightarrow \text{NO}^+(X^1\Sigma^+, v=0) + e^-$  (full circle) can be described in the low-energy range by a  $E^{-0.89}$  dependence, which is fairly close to the  $E^{-1}$  dependence given by the Wigner law [29]. Above 2 eV one observes a rapid fall off that might be connected to the opening up of two competing processes to the AI mechanism, namely,  $\text{N}^+(^3P) + \text{O}^-(^2P) \rightarrow \text{N}(^4S) + \text{O}(^4S) + e^- - 0.54$  eV and of the electron detachment  $\text{N}^+(^3P) + \text{O}^-(^2P) \rightarrow \text{N}^+(^3P) + \text{O}(^3P) + e^- - 1.46$  eV. The curve corresponding to  $\text{N}^+(^1D) + \text{O}^-(^2P) \rightarrow \text{NO}^+(X^1\Sigma^+, v=0) + e^-$  (open circle), appears to exhibit a much shallower slope, namely,  $E^{-0.35}$ , as well as a fall off at smaller center-of-mass energies compared with that of the other channel. This shall be taken with great caution, considering the remark above about the choice of the fit for the partial RIP cross sections.

The magnitude of the AI cross sections is of some interest at low energies, even if the absolute numbers should be taken with caution. At 0.1-eV center-of-mass energy, both curves are in the  $10^{-17}$ -cm<sup>2</sup> range for the cross sections. This is particularly interesting because this is much smaller than the upper limit that can be evaluated by the following relation (see Urbain [26]):

$$\sigma_{\text{AI}}(E'_{\text{c.m.}}) = \frac{\pi(N_{\max} + 1)^2 \hbar^2}{2\mu' E'_{\text{c.m.}}}. \quad (17)$$

This assumes that the associative flux is 100% efficient for the ionization. In other words, none of the flux is allowed to give  $A^+ + B^- \rightarrow A^+ + B + e^-$ ,  $A^- + B^+$ , or  $A + B$ . This is certainly true for the two former processes that are (highly) endothermic, but not necessarily true for the latter one. The energy dependent  $N_{\max}$  is defined above and is related to the centrifugal distortion of the potential curve. In the present case, Eq. (17) can be rewritten at the energy of 0.02 eV as follows:  $\sigma_{\text{AI}} + 4.4 \times 10^{-18} (N_{\max} + 1)^2$  cm<sup>2</sup>. The suitable energy dependent  $N_{\max}$  for the  $X^1\Sigma^+$  state is around 220, which gives a cross section of  $2.1 \times 10^{-13}$  cm<sup>2</sup>. This number is four orders of magnitude larger than the one we have extracted from our model [ $\text{N}^+(^3P, ^1D) + \text{O}^-(^2P) \rightarrow \text{NO}^+(X^1\Sigma^+, v=0) + e^-$ ]. Moreover, a recent measure-

ment of the associative-ionization process [30] gave a value of  $1.34 \times 10^{-14}$  cm<sup>2</sup> at 0.02 eV for  $\text{N}^+(^3P, ^1D) + \text{O}^-(^2P) \rightarrow \text{NO}^+ + e^-$ , thus one order of magnitude lower than the upper limit but still three orders of magnitude larger than ours. This apparent contradiction is actually not a real one and everything can be rationalized, since the different experiments (calculations) do not refer to the same final channel. Indeed, while colliding  $\text{N}^+$  with  $\text{O}^-$  [24], the resulting molecular ion can be produced in various electronic and rovibrational states. At 0.02-eV center-of-mass energy, eight different states can be populated:  $X^1\Sigma^+$ ,  $a^3\Sigma^+$  [both correlating to  $\text{N}(^4S) + \text{O}(^4S)$ ], but also  $b^3\Pi$ ,  $w^3\Delta$ ,  $b'^3\Sigma^-$ ,  $A'^1\Sigma^-$ ,  $w^1\Delta$ , and  $A^1\Pi$  [all correlating to  $\text{N}^+(^3P) + \text{O}(^3P)$ ]. To conclude, the useful information we extracted from our model is that the  $X^1\Sigma^+$ ,  $v=0$  state is a minor product in the associative-ionization process.

## VI. CONCLUSION

The resonant ion-pair formation  $\text{N}^+(^3P, ^1D, ^1S) + \text{O}^-(^2P)$  resulting from the recombination of  $\text{NO}^+(X^1\Sigma^+, v=0)$  with electrons has been studied over the electron-energy range 8–18 eV. Our data contains structures, in particular a sharp peak at 12.44 eV. The data are compared with those of Erman *et al.* [22] obtained by photoionization of  $\text{NO}(X^2\Pi_r)$ . The differences are rationalized, especially as they relate to the selection rules and the differences in the Franck-Condon regions.

The dissociative recombination of  $\text{NO}^+$  and the resonant dissociative excitation [(RDE) occurs below the threshold for direct dissociative excitation] involve stabilization of the same excited states in NO, which means that one would expect some correlations between the DR, RDE, and RIP cross sections. Indeed, the DR and RDE cross sections show enhancement in the energy region 8–18 eV [8]. However, the magnitude of the RIP cross section is only a few percent of the total DR and RDE cross sections.

A simple model was applied to extract the cross sections for the AI process and some interesting perspective came out of it, while comparing it with a recently performed measurement by Naji *et al.* [27]. From our measurement, it turns out that the ground-state  $\text{NO}^+$  molecular ion is a minor product of the AI process.

## ACKNOWLEDGMENTS

We are thankful to the staff of the Manne Siegbahn Laboratory for valuable help with the experiment. One of us (A. L. P) would like to acknowledge discussions with A. Suzor-Weiner and E. Ferguson, as well as with X. Urbain, with whom a very fruitful collaboration was established on the study of the associative-ionization process during a six months visit in Louvain La Neuve. This work was supported by the Swedish Foundation for International Cooperation in Research and Higher Education (STINT), the Swedish Natural Science Research Council (NFR), and the Göran Gustafsson Foundation. N. D. and D. P. were supported in part by the Office of Fusion Energy of the U.S. Department of Energy under Contract No. DE-A105-95ER54293 with the National Institute of Standards and Technology.

- [1] W. Zong, G. H. Dunn, N. Djurić, M. Larsson, A. Al-Khalili, A. Neau, A. M. Derkatch, L. Viktor, W. Shi, A. Le Padellec, S. Rosén, H. Danared, and M. af Ugglas, *Phys. Rev. Lett.* **83**, 951 (1999).
- [2] V. I. Shematovich, D. V. Bisikalo, and J. C. Gerard, *J. Geophys. Res.* **99**, 23217 (1994).
- [3] F. L. Walls and G. H. Dunn, *J. Geophys. Res.* **79**, 1911 (1974).
- [4] P. M. Mul and J. Wm. McGowan, *J. Phys. B* **12**, 1591 (1979).
- [5] E. Alge, N. G. Adams, and D. Smith, *J. Phys. B* **16**, 1433 (1983).
- [6] T. Mostefaoui, S. Laubé, G. Gautier, C. Rebrion-Rowe, B. R. Rowe, and J. B. A. Mitchell, *J. Phys. B* **32**, 5247 (1999).
- [7] C. S. Weller and M. A. Biondi, *Phys. Rev.* **172**, 198 (1968).
- [8] L. Vejby-Christensen, D. Kella, H. B. Pedersen, and L. H. Andersen, *Phys. Rev. A* **57**, 3627 (1998).
- [9] J. N. Bardsley, *J. Phys. B* **1**, 365 (1968).
- [10] C. M. Lee, *Phys. Rev. A* **16**, 109 (1977).
- [11] H. Sun, K. Nakashima, and H. Nakamura, in *Dissociative Recombination: Theory, Experiment and Applications*, edited by B. R. Rowe, J. B. A. Mitchell and A. Canosa (Plenum Press, New York, 1993), p. 25; also see H. Sun and H. Nakamura, *J. Chem. Phys.* **93**, 6491 (1990).
- [12] G. Ringer and W. R. Gentry, *J. Chem. Phys.* **71**, 1902 (1979).
- [13] S. E. Nielsen and J. S. Dahler, *J. Chem. Phys.* **71**, 1910 (1979).
- [14] J. R. Peterson, A. Le Padellec, H. Danared, G. H. Dunn, M. Larsson, Å. Larson, R. Peverall, C. Strömholm, S. Rosén, M. af Ugglas, and W. J. van der Zande, *J. Chem. Phys.* **108**, 1978 (1998).
- [15] G. Chambaud and P. Rosmus, *Chem. Phys. Lett.* **165**, 429 (1990).
- [16] A. G. Calamai and K. Yoshino, *J. Chem. Phys.* **101**, 9480 (1994); R. Wester, K. G. Bushan, N. Altstein, D. Zajfman, O. Heber, and M. L. Rappaport, *J. Chem. Phys.* **110**, 11830 (1999).
- [17] Å. Larson, N. Djurić, W. Zong, C. H. Green, A. E. Orel, A. Al-Khalili, A. M. Derkatch, A. Le Padellec, A. Neau, S. Rosén, W. Shi, L. Viktor, H. Danared, M. af Ugglas, M. Larsson, and G. H. Dunn, *Phys. Rev. A* **62**, 042707 (2000).
- [18] S. Rosén, A. Derkatch, J. Semaniak, A. Neau, A. Al-Khalili, A. Le Padellec, L. Viktor, H. Danared, M. af Ugglas, R. Thomas, and M. Larsson, *Faraday Discuss.* **115**, 295 (2000).
- [19] A. Neau, A. Al-Khalili, S. Rosén, J. Semaniak, A. Le Padellec, A. M. Derkatch, W. Shi, L. Viktor, M. Larsson, R. Thomas, M. Nagard, K. Andersson, H. Danared, and M. af Ugglas, *J. Chem. Phys.* **113**, 1762 (2000).
- [20] C. Strömholm, J. Semaniak, S. Rosén, H. Danared, S. Datz, W. van der Zande, and M. Larsson, *Phys. Rev. A* **54**, 3086 (1996).
- [21] A. Lampert, A. Wolf, D. Habs, J. Kettner, G. Kilgus, D. Schwalm, M. S. Pindzola, and N. R. Badnell, *Phys. Rev. A* **53**, 1413 (1996).
- [22] P. Erman, A. Karawajczyk, E. Rachlew-Källne, and C. Strömholm, *J. Chem. Phys.* **102**, 3064 (1995).
- [23] NIST Standard Reference Database Number 69, edited by W. G. Mallard and P. J. Linstrom, February 2000, National Institute of Standards and Technology, Gaithersburg MD, 20899 (<http://webbook.nist.gov>).
- [24] G. Herzberg, *Molecular Spectra and Molecular Structure I, Spectra of Diatomic Molecules* (Krieger, Melbourne, FL, 1950).
- [25] H. Oertel, H. Schenk, and H. Baumgärtel, *Chem. Phys.* **46**, 251 (1980).
- [26] X. Urbain, thèse de doctorat, Université de Louvain, 1990.
- [27] A. Naji, K. Olamba, J. P. Chenu, S. Szücs, M. Chibisov, and F. Brouillard, *J. Phys. B* **31**, 2961 (1998).
- [28] Å. Larson and A. E. Orel, *Phys. Rev. A* **59**, 3601 (1999).
- [29] E. P. Wigner, *Phys. Rev.* **73**, 1002 (1948).
- [30] E. A. Naji (private communication).
- [31] D. L. Albritton, A. L. Schmeltekopf, and R. N. Zare, *J. Chem. Phys.* **71**, 3271 (1979).